Supporting Information

Microscale Solid-State Thermal Diodes Enabling Ambient Temperature Thermal Circuits for Energy Applications

Song Wang,[1,2,†] Anton L. Cottrill,[1,†] Yuichiro Kunai,[1] Aubrey R. Toland,[1] Pingwei Liu,[1] Wen-Jun Wang,[2] and Michael S. Strano[1,*]

[1] 77 Massachusetts Ave., Department of Chemical Engineering, Massachusetts Institute of Technology, Cambridge, MA, USA

[2] State Key Lab of Chemical Engineering, College of Chemical and Biological Engineering, Zhejiang University, Hangzhou, China

[†]These two authors contributed equally to this paper

[*]Corresponding author's email address: strano@MIT.edu

1. Thermal Diode Fabrication and Characterization:

Table S1. Formulations and properties of high internal phase emulsion foam

Run	Oil:Water (v/v)	Porosity (%) [a]	Density (g/cm^3) [a]
1	1:5	85.4	0.154
2	1:6	87.0	0.136
3	1:7	88.0	0.126
4	1:9	90.0	0.105
5	1:10	90.7	0.098

[a] Density was obtained by measuring volume and weight at room temperature, and porosity was calculated by assuming skeleton's density was same as polystyrene's density, 1.05 g/cm^3.

Table S2. Transition temperatures of *PFH* with varying porosities and paraffins.

Porosity (%)	85.37[a]	87.05[a]	88.02[a]	90.03[a]	90.71[a]	90.71[b]	90.71[c]
Melting point (℃)[d]	30.3	32.1	31.1	30.8	30.4	20.8	40.0
Freezing point (℃)[d]	26.2	24.5	25.6	26.7	25.9	15.0	32.2
Transition point (℃)[e]	28.2	28.3	28.4	28.8	28.2	17.9	36.1

[a] *PFH-O*. [b] *PFH-H*. [c] *PFH-E*. [d] Determined by DSC. [e] Average of melting point and freezing point.

Table S3. Thermal conductivity of *PFH* and the calculated thickness ratio of PMMA and *PFH*.

Types	Thermal conductivity (W/(m K))		L_B/L_A [b]
	Below T* [a]	Above T* [a]	
PFH-O	0.350	0.167	1.26
PFH-H	0.327	0.170	1.23
PFH-E	0.270	0.160	1.08

[a] Transition point, 28.2 ºC for *PFH-O*, 17.9 ºC for *PFH-H* and 36.1 ºC for *PFH-E* as obtained by DSC. [b] According to the analytical model from Cottrill and Strano, L_B is thickness of *PFH*, L_A is thickness of PMMA. $\frac{L_B}{L_A}=\frac{\sqrt{k_{B1}k_{B2}}}{k_A}$, where we set L_A = 1.6 mm.

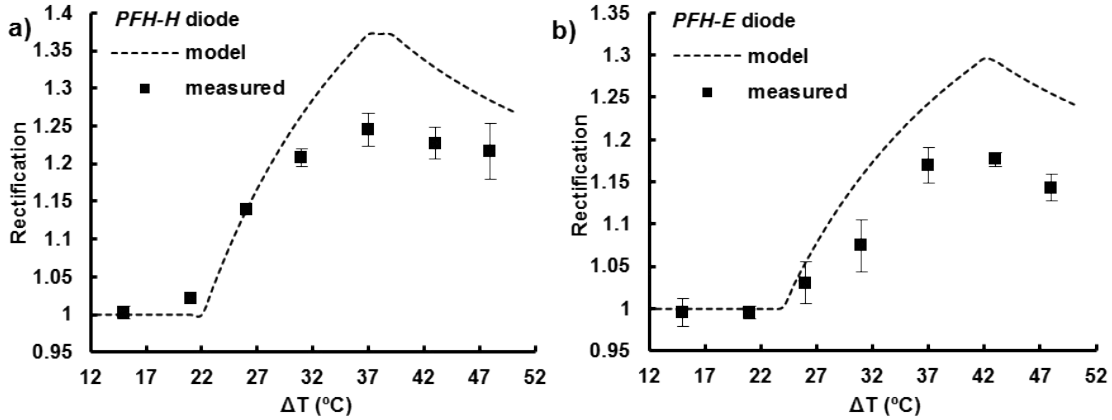

Fig. S1: a) Thermal rectifications obtained via analytical model and heat flux measurements for a thermal diode made of *PFH-H* with varying temperature differences; upper thermoelectric heater was maintianed at 40 ºC. b) Thermal rectifications obtained via analytical model and heat flux mesurements for a thermal diode made of *PFH-E* with varying temperature differences; upper thermoelectric heater was maintained at 60 ºC.

2. Modeling the Thermal Diode Bridge:

The 1-D energy conservation equation for a temperature dependent thermal conductivity and a temperature independent heat capacity is shown in eqn (S1) for the phase change material (PCM) (material B). This conservation equation accounts for the change in thermal conductivity in response to the phase change.

$$\rho_B C_B \frac{\partial T_B}{\partial t} = \frac{\partial}{\partial x_B}\left(k_B(T_B)\frac{\partial T_B}{\partial x_B}\right) \tag{S1}$$

where ρ_B is the density of material B, C_B is the heat capacity of material B, T_B is the spatial and temporal temperature of material B, t is time, x_B is the spatial dimension for material B, and k_B is the thermal conductivity of material B.

For the non-phase change material (material A), the 1-D energy conservation equation assumes constant thermal conductivity and constant heat capacity.

$$\frac{\partial T_A}{\partial t} = \alpha_A \frac{\partial^2 T_A}{\partial x_A^2} \tag{S2}$$

where T_A is the spatial and temporal temperature of material A, x_A is the spatial dimension for material A, and α_A is the thermal diffusivity of material A.

The thermal conductivity of material B is assumed to undergo a smooth step change in response to the phase change, and it is well-represented by an arctan function.

$$k_B = k_{B,0}\left(1 + \frac{2\beta}{\pi}\tan^{-1}\left(\gamma\left(T_B - T^*\right)\right)\right) \tag{S3}$$

where $k_{B,0}$ is the mean thermal conductivity of the two phases for material B, T^* is the transition temperature of material B, γ is an amplification factor that should be sufficiently large in order to represent the smooth step change in thermal conductivity. We assume $\gamma = -5\ K^{-1}$ for all simulations. β is determined by the thermal conductivity of each phase, as described by the following equation for our *PFH-O* thermal diode.

$$\frac{1+\beta}{1-\beta} = \frac{k_{B1}}{k_{B2}} \tag{S4}$$

where k_{B1} and k_{B2} refer to the thermal conductivities of material B below and above the transition point, respectively.

Insertion of eqn (S3) into eqn (S1) yields eqn (S5) for the energy conservation balance for material B.

$$\frac{\partial T_B}{\partial t} = \frac{k_{B,0}\ 2\beta\gamma}{\rho_B C_B\ \pi}\frac{\left(\frac{\partial T_B}{\partial x_B}\right)^2}{1+\gamma^2\left(T_B - T^*\right)^2} + \frac{k_{B,0}}{\rho_B C_B}\left(1 + \frac{2\beta}{\pi}\tan^{-1}\left(\gamma\left(T_B - T^*\right)\right)\right)\frac{\partial^2 T_B}{\partial x_B^2} \tag{S5}$$

It is known that a phase change material operating within proximity to its phase change will have an effective heat capacity associated with the phase change.[S1] However, the model proposed in eqn (S5) assumes a constant heat capacity for material B. This is resolved by maintaining the heat capacity in eqn (S5) as being constant and having its value be equal to the effective heat capacity associated with

the phase change. This is a valid simplification if the temperature fluctuations occur within the melting range of the phase change material,[S1] which is indeed the case for our system, as will be shown.

The effective heat capacity due to the occurrence of the phase change, is given by eqn (S6) and (S7).

$$C_B = C_{B,eff} = C_{B,0}\left(1 + \frac{s\,T_a}{T_m}\right) \tag{S6}$$

$$s = \frac{\varphi h}{2C_{B,0}T_a} \tag{S7}$$

where s is the Stefan number, φ is the mass fraction of the phase change material in a PCM composite, h is the latent heat per mass, $C_{B,0}$ is the standard heat capacity of material B, T_m is the half-width of the melting range for material B, and T_a is the amplitude of temperature oscillations.

At this point, the energy conservation equations for material A and material B have been described. For modeling the thermal bridge diode circuit show in Fig. 4c, the conservation equations for material A and B must be interfaced and form two systems with different orders of boundary conditions.

The boundary conditions are provided in eqn (S8) and (S9). The oscillating boundary conditions (eqn S8) will be applied to the external face of material A for one system and the external face of material B for the other system. Thus, the no heat flux conditions (eqn S9) will be applied to the external face of material B in one system and the external face of material A in the other system.

$$T_{in} = T_0 + T_a sin(\omega t) \tag{S8}$$

where T_0 is the median temperature of temperature oscillations and ω is the angular frequency of temperature oscillations.

$$\frac{\partial T}{\partial x} = 0 \tag{S9}$$

The initial temperature distribution (T_{00}) throughout the device is assumed to be constant and equal to the mean temperature of temperature oscillations (T_0).

This model was solved by discretizing the system in space and solving with the method of lines with ode15s in MATLAB (MATLAB code provided, ‘thermal_diode_main’ and “ODE_configure’). The

parameters used for modeling the thermal diode bridge for our octadecane-based (OD) thermal diode interfaced with polycarbonate (PC) are shown in Table S4. As can be seen from the values of T_a, T_m, T^*, and T_0, the temperature fluctuations occur within the melting range of the phase change material, allowing application of eqn (S6). Experimental support for these values is provided in the following section and Fig. S2a.

Table S4: Parameters used for numerically modeling the thermal diode bridge circuit for our octadecane-based thermal diode described in section 2, as well as for modeling the system described in section 4. References are indicated by brackets. $k_{B2} = 0.17\ W\ m^{-1}\ K^{-1}$ and $k_{B1} = 0.35\ W\ m^{-1}\ K^{-1}$.

$T_a = 5$ ℃	$k_A = 0.2\frac{W}{m\ K}$ [this work] (PC at RT)	$\beta = 0.35$
$T^* = T_0 = T_{00} = 27$ ℃ [S2] (pure OD)	$k_{B,0} = \frac{k_{B2} + k_{B1}}{2} = 0.26\frac{W}{m\ K}$ [this work] (porosity 90.7%)	$\gamma = -5\frac{1}{K}$
$T_m = 5$ ℃ [S2] (pure OD)	$\alpha_A = 0.144\frac{mm^2}{s}$ [this work] (PC at RT)	$\omega = 0.0785\ s^{-1}$
$L_A = 380\ \mu m$	$C_{B,0} = 1600\frac{J}{kg\ K}$ [S2] (pure OD at RT)	$h = 243{,}000\frac{J}{kg}$ [S2]
$L_B = 460\ \mu m$	$\rho_B = 0.777\frac{g}{mL}$ [S2] (pure OD at RT)	$\varphi = 1$ (assume pure OD)

3. Experimental Thermal Diode Bridge Details:

The setup described in Fig. 4c and the experimental section of the manuscript was used to probe the performance of our octadecane-based thermal diodes in the thermal diode bridge circuit. Details of the input temperature oscillations generated by the thermoelectrics wired in parallel are shown in Fig. S2a.

The slope in Fig. S2b is the Seebeck coefficient for the central thermoelectric in Fig. 4c.

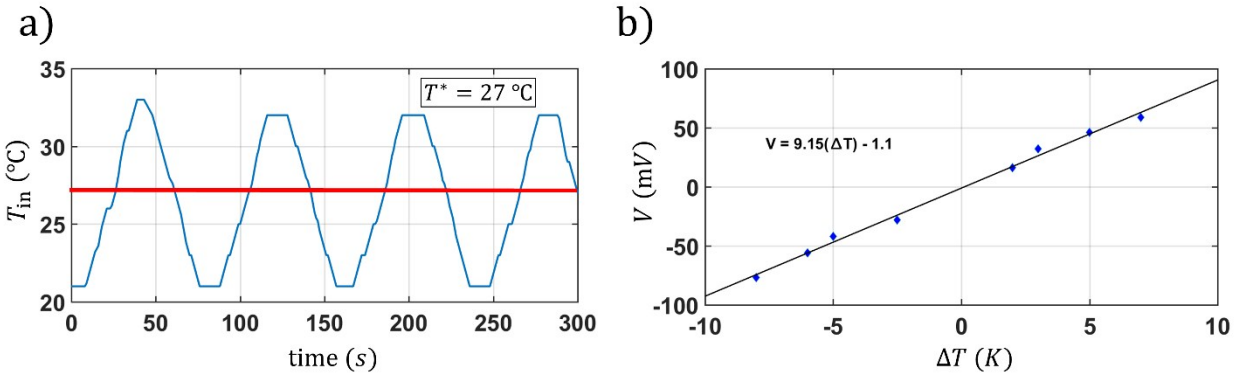

Fig. S2: a) Temperature oscillation data for the input temperature fluctuations (T_{in}) generated by the potentiostat setup (Fig. 4c and experimental section) at an angular frequency $\omega = 0.0785\ s^{-1}$. The median temperature of temperature oscillations (red) occurs at the phase transition temperature of octadecane $(T^* = 27\ °C)$. b) Measurement of the Seebeck coefficient for the center, sensory thermoelectric (Fig. 4c and experimental section). Measurements were obtained by varying the temperature difference using a temperature controlled stage (Echotherm™ chilling/heating dry bath) and forced convection (fan) on either side of the thermoelectric. Temperatures and voltages were acquired with K-type thermocouples and a multimeter, respectively.

The voltage equation shown in eqn (14) assumes open circuit conditions. The voltage equation shown in eqn (S10) assumes closed circuit conditions. As mentioned in the main text, the voltage output data from the central thermoelectric in the thermal circuit in Fig. 4c was converted to a temperature difference according to eqn (14) by assuming a Seebeck coefficient (Γ_S) equal to 1.5 mV K^{-1}. It should be noted that, for the closed circuit measurements, the proper equation to apply to this conversion is eqn (S10). Eqn (14) is the proper equation to apply for open circuit conditions. Therefore, the 1.5 mV K^{-1} "Seebeck coefficient" used to convert the voltage data to a temperature difference for the closed circuit measurements is actually an effective Seebeck coefficient, which is scaled by the internal and external electrical resistances in the system. We have included this discussion for rigor.

$$V = \frac{\Gamma_S \Delta T}{(1 + R_{int}/R_{ext})} \qquad \text{(S10)}$$

where Γ_S is the Seebeck coefficient, ΔT is the temperature difference, V is the voltage, R_{int} is the internal electrical resistance of the thermoelectric, and R_{ext} is the external electrical resistance in the circuit.[S3]

We calculated the internal resistance of our central thermoelectric module to be 1.7 Ω. To obtain this value, we compared open and closed circuit voltages generated by our thermoelectric under identical

temperature biases using a 1.6 Ω external resistor.

4. Analysis of the Effect of Temperature Dependent Heat Capacity:

The experimental data obtained for the thermal diode bridge circuit was compared with an additional model in order to investigate the effect of the variable heat capacity associated with the phase change on the output of the thermal diode bridge.

For this model, the energy conservation equations for the materials A and B are given by eqn (S11) and (S12), respectively.

$$\frac{\partial T_A}{\partial t} = \alpha_A \frac{\partial^2 T_A}{\partial x_A^2} \tag{S11}$$

$$\rho_B C_B(T_B) \frac{\partial T_B}{\partial t} = k_B \frac{\partial^2 T_B}{\partial x_B^2} \tag{S12}$$

Eqn (S12) has been addressed numerically by Richardson and Woods.[S1] The nonlinear nature of the heat transfer model was addressed by solving numerically using the Crank-Nicolson method with variable thermal diffusivity.

Eqn (S12) then becomes:

$$\frac{\partial T_B}{\partial t} = \alpha_B(T) \frac{\partial^2 T_B}{\partial x_B^2} \tag{S13}$$

We addressed this model numerically (MATLAB code provided, 'heat_capacity_T') using the Crank-Nicolson method, as provided in eqn (S14).

$$\frac{T^{n+1}_i - T^n_i}{\Delta t} = \frac{a}{2(\Delta x)^2}\left[\left(T^{n+1}_{i+1} - 2T^{n+1}_i + T^{n+1}_{i-1}\right) + \left(T_{i+1}{}^n - 2T^n_i + T_{i-1}{}^n\right)\right] \tag{S14}$$

i refers to space discretization, n refers to time discretization, Δx is the length of the space discretization, Δt is the step in time.

If in segment A

$$a = \alpha_A \tag{S15}$$

If in segment B and $T < T^* - T_m$ or $T > T^* + T_m$

$$a = \frac{k_{B,0}}{\rho_B C_{B,0}} \tag{S16}$$

If in segment B and $T^* - T_m \leq T \leq T^* + T_m$

$$a = \left(\frac{k_{B,0}}{\rho_B C_{B,0}}\right)\left(1 + \frac{s\,T_a}{T_m}\right)^{-1} \tag{S17}$$

With small enough step size, we can assume $a_i^n = a^{n+1}{}_i$ in order to ensure linearity and solve the system of equations.

We use the following boundary conditions for insertion into the scheme above:

$$T_N^n = T_{N-1}{}^n \text{ (no flux)} \tag{S18}$$

where i = N is the grid point at the output of the thermal diode bridge.

$$T_1^n = T_0 + T_a \sin(\omega t_n) \tag{S19}$$

where i = 1 is the grid point at the input of the thermal diode bridge.

The initial temperature distribution (T_{00}) throughout the device is assumed to be constant and equal to the mean temperature of temperature oscillations (T_0).

The model in eqn (S11) to (S19) was analyzed with the parameters in Table S4 to determine whether the independent effect of the change in heat capacity - due to the phase change – could result in rectification of the oscillatory temperature input. Two analyses were performed: 1) varying the temperature oscillation amplitude for a given transition temperature $(T^* = 27\ ^\circ\text{C})$ 2) varying the transition temperature for a fixed temperature oscillation amplitude $(T_a = 5\ ^\circ\text{C})$. These conditions were chosen such that the variable thermal diffusivity would be activated (i.e., temperatures outside and within the melting range are accessed) and such that the symmetry between the median oscillation temperature and phase transition temperature were broken. The results of these analyses are shown in Fig. S3a and S3b, respectively.

The results in Fig. S3a show that the increase in temperature amplitude has no effect on the thermal circuit's ability to rectify, which is shown by the double polarity temperature difference that symmetrically oscillates around a value of zero. The sole effect of the increase in temperature amplitude is to introduce additional kinks in the temperature difference profile, which are related to the different time scales for standard thermal diffusion and phase change front movement.

The results in Fig. S3b show that slight rectification is possible by breaking the symmetry between the median temperature of oscillations and the phase transition temperature (i.e., $T_0 \neq T^*$). These constraints also introduce kinks into the temperature difference profiles, which are similar to those observed in Fig. S3a. The model discussed in the manuscript and section 2 accurately accounts for the unsteady thermal rectification of our thermal diode bridge circuit for a variety of reasons. First, kinks are not observed in our experimental temperature difference profiles. Second, as shown in Fig. S2a, our experimental temperature input matches very well with our model inputs in section 2. For example, the median temperature of oscillations is essentially the transition temperature for our phase change material, octadecane. At any rate, the results of Fig. S3b clearly indicate that rectification can be achieved by breaking the symmetry between T_0 and T^*. The researchers do not believe this is the mechanism for the experimental output shown in Fig. 4d; however, the data of Fig. S3b provide insight for further development of the thermal diode bridge circuit.

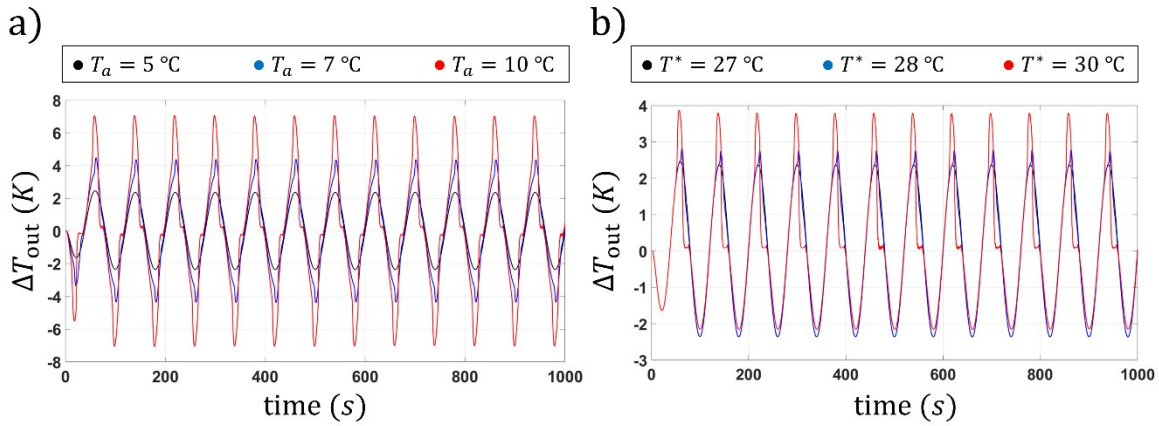

Figure S3: An analysis of the effect of temperature oscillation amplitude (a) and phase transition temperature (b) on the output of a thermal diode bridge modeled by eqn (S11) to (S19). All parameters used for the simulations are in Table S4, unless otherwise indicated.

5. FFT Analyses of the Thermal Diode Bridge Circuit:

The Fast Fourier Transforms (FFTs) for our thermal diode bridge circuit experimental outputs (Fig. 4d, red and blue) are shown in Fig. S4a (open circuit) and S4b (closed circuit). As mentioned in the manuscript, the outputs (Fig. 4d) are characterized by dynamic thermal rectification. Of note is that the FFTs for these experimental outputs are characterized by a standard harmonic series. Furthermore, the model proposed (SI section 2) for the dynamic rectification (Fig. 4d, dashed black) is also characterized by a standard harmonic series, as shown in Fig. S4c. We also note that the second harmonic in the FFT

is critical for the observation of thermal rectification. We postulate, and this can be easily confirmed, that the even numbered harmonics, in particular, are important for shifting the input temperature oscillations, such that single polarity output is observed.

The FFTs in Fig. S4d to S4f correspond to the models in Fig. S3a (S3b) (black), Fig. S3a (red), and Fig. S3b (red), respectively. The data in Fig. S3a (S3b) (black) and Fig. S3a (red) are not characterized by dynamic thermal rectification. The FFTs in Fig. S4 reflect this also. For the FFT in Fig. S4d, a single peak is observed – related to the input driving frequency – as anticipated for a linear thermal circuit characterized by a single thermal diffusivity (T_a and T_m dictate that all temperature oscillations occur within melting range for this case, hence a single thermal diffusivity). For Fig. S4e, only odd-numbered harmonics are observed. Again, even-numbered harmonics, which we postulate as being critical for dynamic thermal rectification are missing in the FFT, as is dynamic thermal rectification in Fig. S3a (red). However, for the FFT in Fig. S4f, we observe a standard harmonic series – characteristic of dynamic thermal rectification – which matches with the dynamic thermal rectification results in Fig. S3b (red).

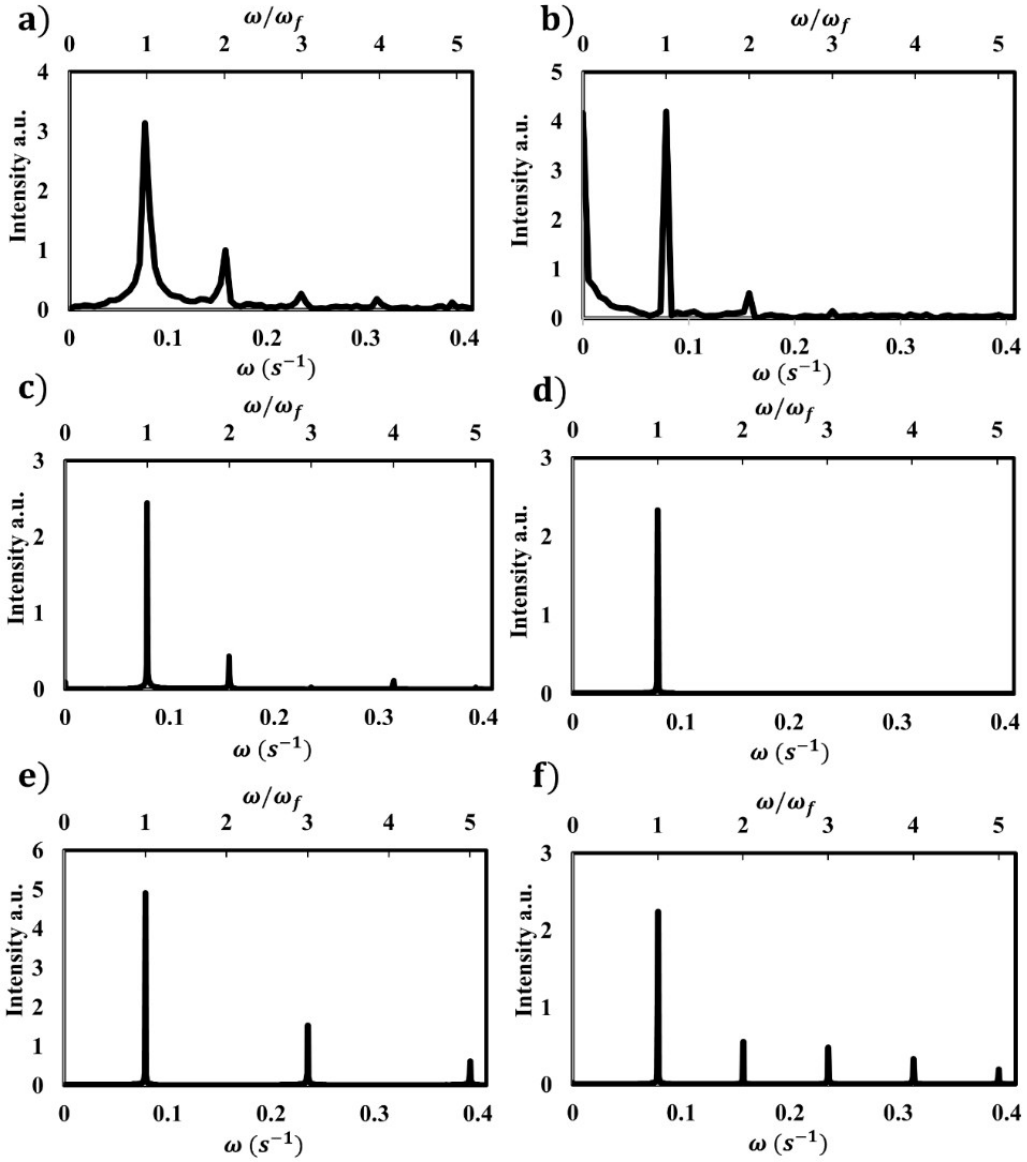

Fig. S4: a) FFT for the open circuit (blue) experimental data in Fig. 4d as a function of angular frequency. ω_f refers to the funadamental driving frequency (0.0785 s^{-1}) for the thermal circuit. b) FFT for the closed circuit (red) experimental data in Fig. 4d as a function of angular frequency. c) FFT for the theoretical data (dashed black) in Fig. 4d as a function of angular frequency. d) FFT for the theoretical data (black) in Fig. S3a and S3b as a function of angular frequency. e) FFT for the theoretical data (red) in Fig. S3a as a function of angular frequency. f) FFT for the theoretical data (red) in Fig. S3b as a function of angular frequency.

6. Experimental Temperature Difference Output and FFT for a Linear System:

Using the experimental setup described in Fig. 4c, we probed the performance of a linear thermal circuit, as discussed in eqn (6)-(8) and Fig. 4a. The results are shown in Fig. S5 for the same input driving frequency as used in Fig. 4d. The output is clearly bipolar and symmetric around zero (red line), and the FFT (Fig. S5b) shows a single peak, which corresponds to the driving frequency. This

experiment and its results serve as a control for the experimental setup and illustrate the characteristics of a linear thermal circuit, as described in the manuscript.

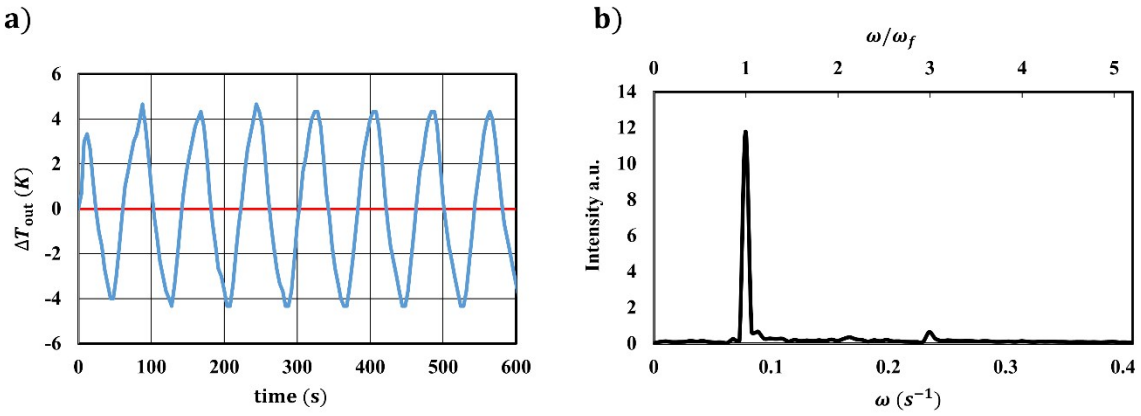

Fig. S5: a) Temperature difference output for a linear thermal circuit using the experimental setup described in the experimental section and Fig. 4c. The angular temperature oscillation frequency is $\omega = 0.0785\ s^{-1}$. Linear thermal masses (1: 3.2 mm polycarbonate; 2: 4.9 mm steel) were situated on either side of the central thermoelectric in lieu of the thermal diodes, as shown in eqn (6)-(8) and Fig. 4a. The experimental output is translated to a temperature difference using a Seebeck coefficient ($\Gamma_S = 3\ mV\ K^{-1}$). b) FFT for the temperature difference output shown in Fig. S5a. The fundamental frequency is the same as the driving frequency, $\omega_f = 0.0785\ s^{-1}$.

References:

S1 M. J. Richardson and A. W. Woods, *Proc. R. Soc. London A Math. Phys. Eng. Sci.,* 2008, **464**, 1029-1056.

S2 C. Vélez, M. Khayet and J. M. Ortiz de Zárate, *Appl. Energy,* 2015, **143,** 383–394.

S3 Paul, D. *Thermoelectric Energy Harvesting Ch. 4* (Intech, 2014).